Materials Science & Engineering A 735 (2018) 73–80

Contents lists available at ScienceDirect

Materials Science & Engineering A

journal homepage: www.elsevier.com/locate/msea

Anti-aging treatment of nuclear power plant steel

Yan Zhao[a], Binyan He[a], Sébastien Saillet[b], Christophe Domain[b], Patrick Le Delliou[b], Michel Perez[c], Rongshan Qin[a,*]

[a] School of Engineering & Innovation, The Open University, Walton Hall, Milton Keynes WA76AA, United Kingdom
[b] EDF R&D Département Matériaux et Mécanique des Composants, Avenue des Renardières – Ecuelles, F-77818 Moret sur Loing, France
[c] Univ. Lyon, INSA-Lyon MATEIS UMR CNRS 5510, F-69621 Villeurbanne Cedex, France

ARTICLE INFO

Keywords:
Duplex stainless steel
Aging
Charpy impact test
External electric field

ABSTRACT

Duplex stainless steel loses impact toughness quickly during its service at nuclear power plant station as pipe and boiler. Aging induced spinodal decomposition in ferrite phase is the mechanism behind this degradation. This work uses electropulsing to treat the aged steel at the service temperature. The charpy impact toughness and Vickers micro-hardness were recovered significantly. Thermoelectric power is recommended to measure the degree of spinodal decomposition in the aging processing, which was recovered by > 83% by the electropulsing treatment. It was proved that the anti-aging treatment was not due to the Ohm heating. Instead, the electropulsing-induced extra free energy change of − 891 J/mol provided thermodynamic driving force for the regeneration processing. Electropulsing-enhanced diffusivity enables the anti-aging processing to be completed quickly.

1. Introduction

Many engineering alloys are in non-equilibrium or metastable states, which evolve toward the equilibrium state during service [1]. The non-equilibrium microstructures are often desirable due to their supreme mechanical properties [2,3], while the non-equilibrium to equilibrium transformation causes the degradation of the materials [4]. The transformation happens from seconds to years depending on the nature of the transition and environmental conditions [5,6]. There are significant research activities to predict the structural transformation from non-equilibrium to equilibrium states [7,8]. A number of strategies to control and to retard the transformation have been developed [9,10]. From the thermodynamic point of view, reversing the structure transformation is possible if sufficient negative free energy flux is injected into the system. External field can be the source to generate the required negative free energy.

The non-equilibrium to equilibrium microstructural transformation can be described in analogy to that of crystallization in an amorphous alloy [11]

$$U = U_0 exp\left(-\frac{V}{k_B T}\right)\left[1-exp\left(-\frac{\Omega}{k_B T}\right)\right] \quad (1)$$

where U is the microstructural transformation rate. The pre-exponential factor U_0 is related to interatomic distance and atomic vibration frequency. k_B is Boltzmann's constant. T is temperature. V is kinetic barrier and Ω is thermodynamic driving force. Retardation of the microstructural transformation can be achieved by increasing kinetic barrier (V) and/or decreasing thermodynamic driving force (Ω). It can be seen from Eq. (1) that the transformation rate becomes negative ($U<0$) when $\Omega<0$. This means that the microstructure transforms toward the reverse direction when the free energy sequence is altered. The reversal transformation causes the regeneration of microstructure and hence the properties.

Gibbs free energy (G) describes the state transformation in materials at constant pressure. By ignoring the contribution from strain-stress energy, the system free energy consists of chemical free energy (G_c), interface energy (G_i) and external field energy (G_e). This can be represented as

$$G^s = G_c^s + G_i^s + G_e^s \quad (2)$$

where the super-index represents state, i.e., $s = n$ the non-equilibrium state and $s = e$ the equilibrium state. The thermodynamic driving force is defined as

$$\Omega = G^n - G^e = (G_c^n - G_c^e) + (G_i^n - G_i^e) + (G_e^n - G_e^e) = \Delta G_c + \Delta G_i + \Delta G_e \quad (3)$$

The external field in the present work is introduced to drive the microstructure regeneration. The transformation from non-equilibrium

* Corresponding author.
E-mail address: rongshan.qin@open.ac.uk (R. Qin).

https://doi.org/10.1016/j.msea.2018.08.023
Received 4 July 2018; Received in revised form 8 August 2018; Accepted 9 August 2018
Available online 10 August 2018
0921-5093/

state to equilibrium state without the external field requires $\Delta G_c + \Delta G_i > 0$. The microstructural regeneration ($\Omega < 0$) demands

$$\Delta G_e < -(\Delta G_c + \Delta G_i) \quad (4)$$

This work aims to use electric current to regenerate the microstructure and properties of duplex stainless steel. Some experimental observations reported in literature hint the possibility of regeneration using electric current. Firstly, the electric-current-induced retardation of precipitation has been observed experimentally in AI-4.1 wt% Cu, Al-1.8 at% Cu and AI-3.3 at% Mg [12], Al-2.7 at% Ag [13], AI-5.6 at% Zn [14] and Al-2Mg-2Zn alloy [15]. The only exceptional report of electropulse-enhanced precipitation was in Al-Cu alloy [16]. This has since been double checked by Onodera and proved to be incorrect [12]. It is well-known that electric-current enhances the mobility of atoms and dislocations and reduces kinetic barrier for microstructural transformation [17,18]. The retardation of precipitation implies the electropulse-reduced thermodynamic driving force. Secondly, electropulse-induced precipitate dissolution has been reported in Mg-9Al-1Zn alloy [19] and 316 L stainless steel [20]. These provide experimental indications that electropulse might reverse thermodynamic driving force in precipitates growth. Our theoretical prediction and numerical calculations have confirmed this possibility [21,22].

Aging is a typical microstructural transformation from non-equilibrium to equilibrium states. The cast duplex stainless steel (DSS) is implemented in many nuclear power plants across the world. This material undergoes solute decomposition and precipitates during aging. The mechanical properties, especially the charpy impact toughness, reduce drastically after aging. The precipitation in this steel has been studied intensively [23]. The solute decomposition has been well characterized and modelled [24–26]. Spinodal decomposition happens firstly in the aging processing, followed the formation and coarsening of G-phase and other precipitates. The aim of the present work was to regenerate the microstructure and mechanical properties of DSS which was caused by the early stage aging (with aging time up to 10,000 h at aging temperature up to 400 °C).

2. Experiments

The chemical compositions of the materials considered in the present work are presented in Table 1. The steel was casted under deliberated processing conditions to consist of ferrite and austenite phases without the formation of any precipitates. The cast was cut into blocks and each block was aged by EDF on laboratory furnaces at defined aging conditions before sending to the Open University for regeneration treatment. The aging conditions for five types of samples are presented in Table 2. The as-received samples were in different dimensions with length > 84 mm, depth > 30 mm and height > 60 mm. The samples were further cut into more than 10 blocks, each with a dimension of $12 \times 12 \times 60\ mm^3$ for electropulsing treatment. The treated samples and some as-received/untreated samples were tested by charpy-U impact. These charpy testing was carried out at RKP450 machine using 450 J nominal energy of the pendulum sheep according to standard NF EN ISO 148–1 and EN ISO 14556.

In order to check the microstructure evolution in electropulsing treatment, samples before and after the electropulsing treatment were prepared for optical microscopy (OM), scanning electron microscopy (SEM), electron back-scattering diffraction (EBSD), transmission electron microscopy (TEM), energy diffraction spectrum (EDS) characterizations and Vickers micro-hardness testing. The thermoelectric power (TEP) of as-received samples and electropulsing treated samples were measured in order to compare to TEP evolution during thermal aging. The change of the TEP coefficients after electropulsing treatment indicates the effect of regeneration. TEP is sensitive to the solute distribution in the material.

Table 2
Aging conditions of the as-received samples.

Sample name	D862	D861	D999	D979	D989
Aging temperature (°C)	400	400	400	325	350
Aging time (hours)	300	1000	10,000	10,000	10,000

Two electropulsing facilities were implemented to treat the samples for regeneration purpose. Both facilities have pulse frequency range from 1 Hz to 1000 Hz and pulse duration from 20 μs to 1000 μs. One pulse generator has peak current up to 200 A and another up to 4000 A, both are adjustable continuously. The selection of pulse instead of continuous current is to minimize the Ohm heat. The pulse wave is in square shape. The smaller current facility was used to treat the small samples to find the adequate treatment parameters. The bigger current facility was implemented to treat the large sample for charpy impact testing. The samples were treated in the same temperature as that in aging process. This was achieved by putting the samples into a resistance furnace. The samples were connected to electropulse generator using copper wires. Thermocouple were embedded into the samples to monitor the real-time temperature caused by furnace heating and Ohm heat. The electropulse facility has been implemented to process the solid and liquid steels in previous studies [27,28].

3. Results

3.1. Characterization of as-received samples

The equilibrium phase diagram of the steel with chemical compositions listed in Table 1 has been calculated using MTDATA commercial thermodynamics software with TCFE4 database. The result is presented in Fig. 1(a). It can be seen that the material at equilibrium state contains face-centered-cubic (fcc) austenite phase, body-centered-cubic (bcc) ferrite phase and several other types of precipitates. Experiments reveal that many precipitates are formed at higher temperature and/or longer aging time in comparison with the spinodal decomposition and G-phase [23–26]. Fig. 1(b) illustrates the metastable phase diagram in a constrain of only liquid, fcc and bcc phases are considered. Two types of bcc crystals (as labels as phases 3 and 4 in Fig. 1(b)) appear when the temperature is lower than 830 K. This is considered as the spinodal decomposition of the original bcc crystal. The decomposition forms a bcc phase containing very high content of Cr, as shown in Fig. 1(c), which leaves the original bcc phase with poor Cr constitution, as shown in Fig. 1(d). The formation of G-phase accompanies with segregation of Ni elements. These have been validated by experimental observations using atom probe tomography microscope (APT) for the steel considered in the present work [24].

The microstructure of as-received samples was examined by various methods. Five types of aged samples show similar phase distribution and grain morphology. The various aging conditions seem to have no observable effects on the microstructure in grain scale. Fig. 2(a) presents the optical image of D999 sample etched by a mixture of 45 g ferric chloride, 9 g copper ammonium chloride, 150 ml hydrochloric

Table 1
Chemical compositions of the cast duplex stainless steel in wt%.

Fe	C	Co	Cr	Cu	Mn	Mo	N	Ni	P	S	Si
Balance	0.033	0.020	21.700	0.020	0.850	2.410	0.032	10.300	0.028	0.001	1.010

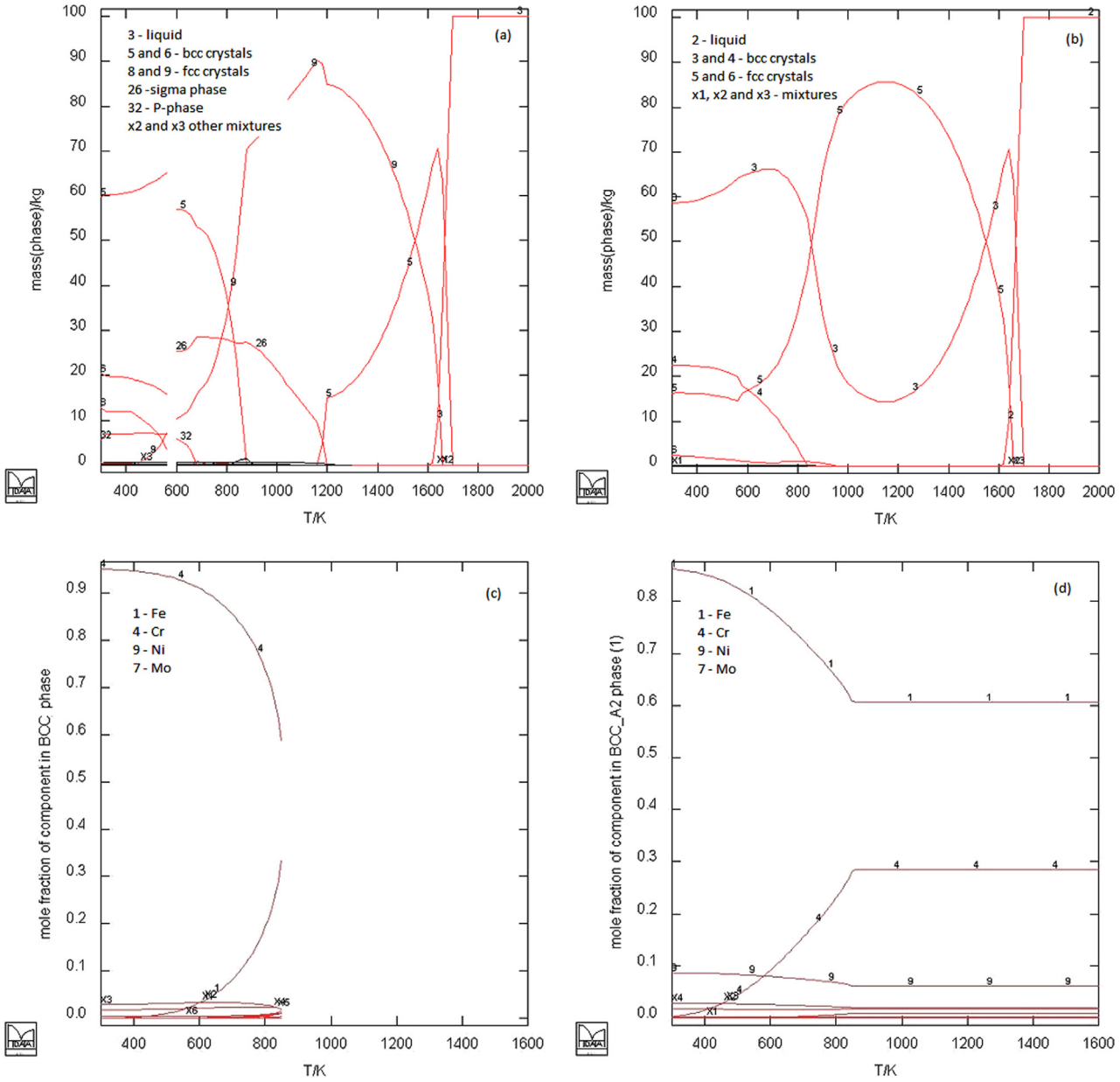

Fig. 1. (a) Equilibrium phase diagram of the alloy calculated by MTDATA commercial software and TCFE4 database using the chemical compositions listed in Table 1; (b) Metastable phase diagram considered only the liquid, fcc and bcc phases; (c) and (d) Chemical compositions in two bcc phases after aging-induced spinodal decomposition.

acid and 75 ml distilled water. The image shows large dendrite grains embedded in the matrix. EBSD image, Fig. 2(b), reveals that the dendrite is austenite phase and the matrix is ferrite. The volume fraction of ferrite accounts for 30%. This is in agreement with the instruction provided by the materials provider EDF. Fig. 2(c) is the SEM image of the as-received material. The SEM sample was not etched. No precipitates particles were observed in the dendrite and matrix. Fig. 2(d) is the TEM image of the as-received samples. The TEM specimens were mechanically polished to a thickness of around 30 μm, punched into 3 mm diameter disks, electrically polished in a solution mixed by 30 ml perchloric acid and 270 ml acetic acid. The acceleration voltage was 200 kV. No precipitates were found in TEM observations. In summary, Fig. 2 supports the viewpoint that the aging treatment at the conditions listed in Table 2 didn't cause the precipitation. The EDS study confirms that the chemical compositions of Cr and Mo in ferrite phase are higher than that of average in materials while the Ni composition is higher in austenite phase. A slightly higher Cr and lower Ni were noticed in the as-received sample than that reported from the alloy provider (Table 1) according to our EDS characterization. According to our calculation, these differences are unlikely to cause observable difference in phase diagram.

However, aging-induced spinodal decomposition and G-phase formation has been confirmed by APT characterizations by another EDF sponsored research project [24]. Some of the co-authors in the present study also got involved in that project and relevant publications. The microstructure alteration in spinodal decomposition is via solute redistribution rather than the crystallographic or phase transformations. The spatial scale is in a few nanometers. The SEM and TEM are not suitable to characterize the microstructure evolution in spinodal decomposition. The APT and TEM study of duplex stainless steel by Matsukawa et al. reveals that the G-phase was detectable only after 10,000 h of aged sample in the crystallographic analysis using TEM [29].

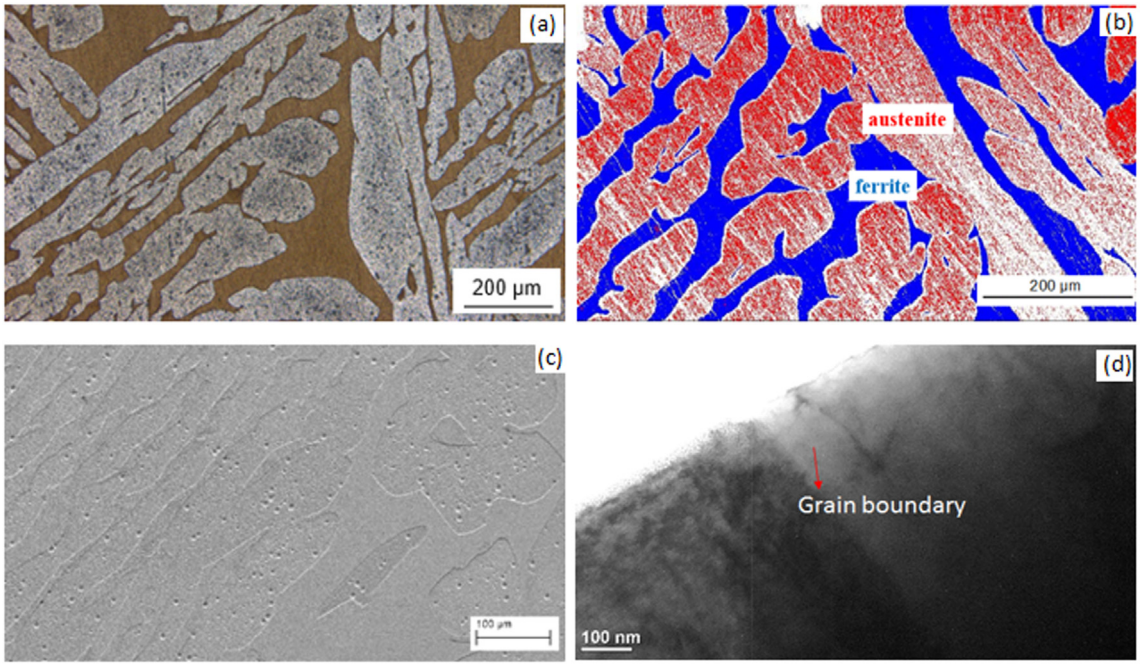

Fig. 2. Microstructure characterization of the as-received D999 sample: (a) Optical microscope image shows the dendrite grain; (b) EBSD image reveals 30% ferrite matrix and 70% austenite phase; (c) SEM image and (d) TEM images reveals no precipitates formation.

3.2. Characterization of spinodal decomposition

Several methods are available to detect the spinodal decomposition in stainless steels, and those methods have been reviewed comprehensively by Lo et al. [30]. These include the acoustic method that measures the change in the longitudinal wave velocity due to the change of lattice parameter of ferrite phase [31], anodic and polarisation method to detect the Cr-rich and Fe-rich areas [32], electrical property method [33], TEP variation method [34], embrittlement measurement method [35], automated ball indentation method [36], magnetic method by measuring the coercive force [37] magnetic transition temperature [38] and AC magnetic susceptibility [39], etc. TEP measurement is a convincing method to detect spinodal decomposition in ferrite. TEP increases with the ferrite content. The higher the ferrite content, the higher the TEP. TEP is affected by Cr and Ni compositions as well [34]. Increasing the contents of Cr and Ni reduces TEP value. TEP is largely related to the electron density of states at the Fermi level. The electron density of states can be measured by X-ray photoelectron spectroscopy (XPS). Fig. 3 is the TEP vs aging time for the considering steel aged at various temperatures. TEP measurement is an excellent indicator of degree of thermal aging. Its value increases along with the aging time. The TEP of the as-received aged samples, according to measurement, are D861: −0.718 μV/°C, D989: −0.587 μV/°C, D999: −0.207 μV/°C, D979: −0.938 μV/°C and D862: −1.0 μV/°C, respectively.

3.3. Regeneration by electric-current-pulses

Samples with dimensions of 30 × 10 × 1 mm^3 were cut from the as-received materials, and were treated by electropulsing facilities using the parameters illustrated in Table 3. During the electropulsing treatment, another as-received sample was put next to the electropulsing treatment sample in the furnace at same duration but without electric current passing through. This is to make sure both samples to experience same thermal treatment. The TEP value of the samples without electropulsing treatment was found the same as that of as-received. Fig. 4 presents the measurement results. It can be seen clearly that electropulsing treatment has reduced the TEP value of the materials.

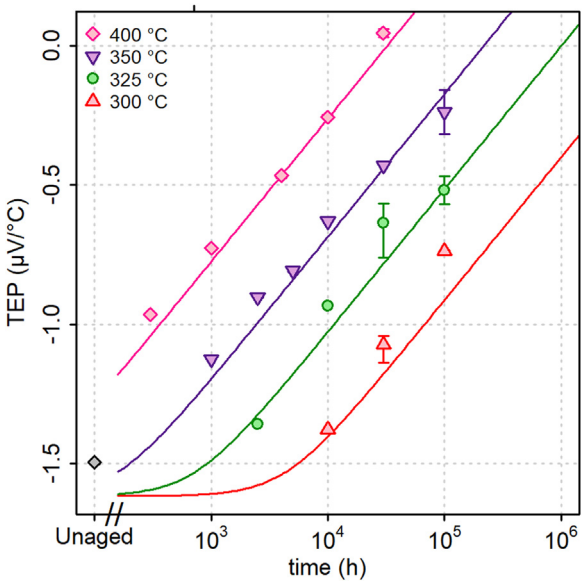

Fig. 3. Thermoelectric power (TEP) vs. aging time for the samples aged at various temperatures.

According to Fig. 3, the lower TEP value corresponding to shorter aging time. By mapping the measured TEP value to the relationship between TEP and aging time, the equivalent aging time after the electropulsing treatment was extracted and presented in Table 4. The regeneration effect was evaluated by the following equation

$$Regeneration\ effect = \frac{t_b - t_a}{t_b} \times 100\% \quad (5)$$

where t_b is the equivalent aging time according to the measured TEP value for the samples without electropulsing treatment, which is found in agreement with the true aging time. t_a is the equivalent aging time according to the measured TEP value after electropulsing treatment. It can be seen that even the least regeneration is still > 83%. For most of samples, the regenerations are over 90%. Please note that the unit of

Table 3
Electropulsing treatment conditions.

Samples	Frequency (Hz)	Pulse duration (μs)	Current density (A/m^2)	Treatment time (h)	Temperature (°C)
D862	100	120	1.3×10^7	1	400
D861	100	200	1.0×10^7	1	400
D999	100	200	1.0×10^7	1	400
D979	100	200	1.3×10^7	1	325
D989	100	120	1.7×10^7	1	350

TEP value in Fig. 4 is nV/°C, while in Fig. 3 is μV/°C. It can be calculated that repeatedly electropulsing treatment under an assumption of each treatment to achieve 80% regeneration rate could extend the service time of the steel components for a factor of almost 9. This has significant potential to extend the service life of steel parts in nuclear power plant.

Vickers micro-hardness has been measured using Struers Duramin-A300 tester at a load of 100 g (therefore, HV0.1). As spinodal decomposition only takes place in ferrite phase, therefore, Vickers hardness was only measured in ferrite regions. The samples were grinded, polished and then etched for 8 s using a solution containing 45 g ferric chloride, 9 g copper ammonium chloride, 150 ml hydrochloric and 75 ml distilled water. Ferrite can be easily allocated. Each sample was tested in 30 different positions in ferrite phases. The average value over all the 30 tests, the top 15 highest values and top 10 highest values were selected to represent the micro-hardness of ferrite. The results for all the samples before and after the electropulsing treatment are presented in Table 5. Electropulsing treatment has reduced the Vickers hardness of the ferrite significantly, and the values are comparable to that of the samples without aging.

In order to prepare the samples for charpy impact testing, same treatment conditions have been implemented to samples with dimensions of $12 \times 12 \times 60\,cm^3$. To achieve the similar electric current density, another electropulsing facility located in 3rd party with peak current up to 4000 A was implemented for the electropulsing treatment. Then Charpy-U specimens were machined and tested. Some of the results are demonstrated in Fig. 5. The figure also included the charpy impact testing results for the unaged samples. It can be seen that electropulsing treatment has recovered the impact toughness of the steels significantly. The mechanical properties of the samples have been regenerated considerably by the electropulsing treatment. However, Fig. 5 also shows some fluctuation results of the electropulsing treatment. This was due to the electropulsing facility at the 3rd party was fabricated for another metallurgical purpose and the electrodes are difficult to manipulate to make contact to the samples inside a furnace.

3.4. Microstructure after electropulsing treatment

The samples after electropulsing treatment have been examined by optical microscope, SEM, EBSD and TEM. In order to make in-situ observation, an inclusion was marked in the samples before electropulsing. The same location was observed for the sample after electropulsing treatment. The optical microscope and SEM images for the samples before and after electropulsing treatments were found identical. EBSD characterization reveals the same pole figures for the samples before and after electropulsing, although electropulsing was reported to be able to rotate the crystal orientations for some other low alloy steel at ambient temperature [40] and change grain morphology as well as the grain size in high carbon steel [41]. The grain morphology and crystallographic orientation were not changed in the present regeneration processing. The possible reason is that the grain size in the samples discussed in the present work is considerably larger and the morphology is dendrite [42].

TEM characterization shows the change of dislocation distribution caused by the electropulsing treatment. Fig. 6 presents the TEM images for D979 samples before and after the electropulsing treatments. There are significant amount of tweed structures presented in the aged samples before electropulsing treatment. This is in agreement with the reported crisscrossing of dislocations in literature [43]. After the electropulsing treatment, those tweed structures disappeared. The large dislocation pileup disappear causes the reduction of the Vickers microhardness. However, this should not be the major reason for the change of the mechanical properties. We believe that the reverse of spinodal decomposition structure is the major reason for the regenerated mechanical properties.

4. Discussion

The recovered TEP value indicates the successful regeneration of the microstructure for the aged samples. The recovered Vickers microhardness and charpy impact toughness confirm the regeneration of the mechanical properties. As was mentioned earlier in this paper, the regeneration demanded the reversed non-equilibrium to equilibrium transformation under electropulsing treatment. This requires the reverse of the system free energy sequence. The change of Gibbs free energy due to electric current is as follows [21]

$$\Delta G_e = \frac{1}{8\pi}\int_v \int_V \frac{\mu^e(r')\vec{j}^e(r')\bullet\vec{j}^e(r') - \mu^n(r')\vec{j}^n(r')\bullet\vec{j}^n(r')}{|r-r'|}drdr' \quad (6)$$

where the superscript e represents the aged (equilibrium) state and n

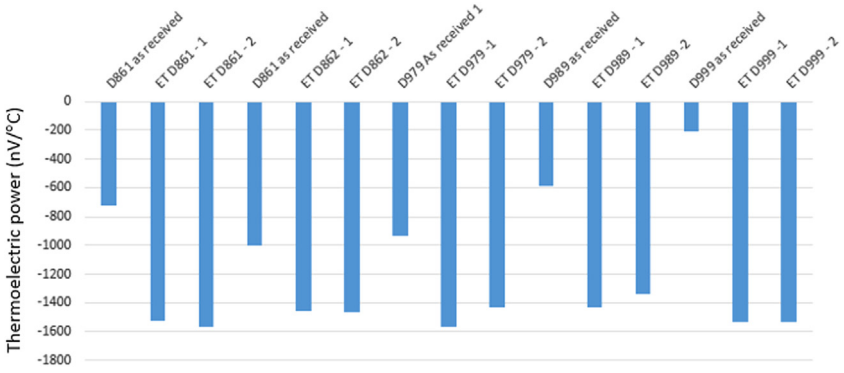

Fig. 4. Measured TEP values for as-received and electropulsing treated (ET) samples.

Table 4
Measured TEP values, corresponding aging time and regeneration efficient.

Sample	D861		D989		D999		D979		D862	
	TEP (μV/°C)	Age (hours)	TEP (μV/°C)	Age (hours)	TEP (μV/°C)	Age (hours)	TEP (μV/°C)	Age (hours)	TEP (μV/°C)	Age (hours)
TEP before EP	− 0.718	1000	− 0.587	10000	− 0.207	10000	− 0.938	10000	− 1.0	300
TEP after EP	− 1.522	< 50	− 1.342	550	− 1.529	100	− 1.566	< 1000	− 1.461	< 50
Regeneration		> 95%		95.5%		99%		90%		> 83%

represents the unaged (non-equilibrium or regenerated) state. μ is the magnetic permeability. j is the current density distribution. r and r' are two different positions within the material. The integration goes throughout the whole samples.

The electric current density distribution can be obtained when the electrical property (electrical conductivity) of all the phases and the configuration of phases in the material are known. The detailed numerical method for calculating this is available in literature [21,44]. The electrical properties of ferrite and austenite phases in steels are available in literature [45]. Many experimental measurements on the evolution of magnetic permeability for duplex stainless steels are reported [38,46]. Aging causes significant reduction of the magnetic permeability. An optimized database regarding to the electric and magnetic properties of stainless steel has been established in this research group and will be published in a separate paper. The spinodal decomposition causes significant change of electrical conductivity distribution in the ferrite phase [44]. The evolution of dislocation in the ferrite phase and the appearance of the solute gradient contributed significantly to the magnetic permeability at the ferrite phase [38].

In order to calculate the Gibbs free energy change due to electric current, the microstructures of aged and regenerated steel have been reconstructed by a phase field method calculation [47]. The interface anisotropic properties of cubic crystals [48] and the relationship between phase field gradient energy and interface anisotropy [49] were implemented. The numerical results were plotted using MatVisual software. The microstructure was reconstructed to possess 70% austenite and 30% ferrite phases in the computational domain. Spinodal decomposition was taken place in ferrite phase. The calculated microstructures for the aged and regenerated steel are presented in Fig. 7. The dendrite grains are austenite. The different colors in austenite grains represent different austenite crystallographic orientation. The matrix is ferrite, in which the different colors representing different Cr compositions. The detailed phase-field calculation will be published in a separate article. In combination with the database for the electric and magnetic properties, it is found that $\Delta G_e = -891\, J/mol$, while the driving force for spinodal decomposition is less than 200 J/mol according to calculation based on a commercial thermodynamic database. The regeneration condition defined by Eq. (4) is satisfied. Electropulsing can drive the aged microstructure to move back to a less aged or unaged state.

Passing electric current pulses to the materials causes temperature increment due to Ohm heat. To calculate the maximum possible temperature change due to the electropulsing treatment, one selected the largest electric current density implemented in the experiments, i.e. $j = 1.7 \times 10^7\, A/m^2$. The equation for calculating the temperature change due to Ohm heat is

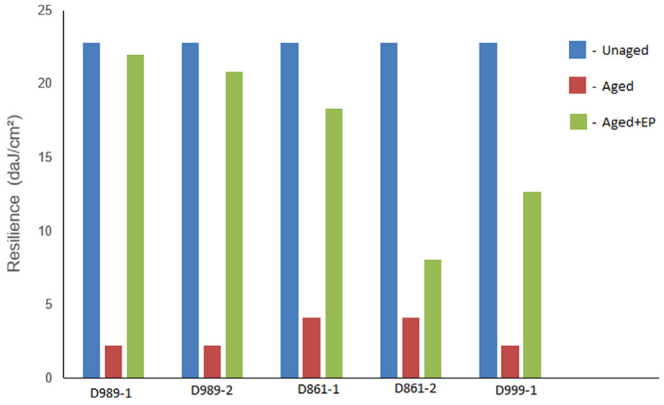

Fig. 5. Charpy test results for unaged, aged and aged + electropulsed samples.

$$\Delta T = \frac{j^2 \rho_e \Delta t}{c \rho_d} \tag{7}$$

where ρ_e is the electrical resistivity of the material, Δt the pulse duration, c the specific heat and ρ_d the mass density. For the sample and electropulsing treatment in the present work, one uses $\rho_e = 9.58 \times 10^{-8}$ Ω·m, $c = 450$ J/kg/K, $\rho_d = 7.8 \times 10^3$ kg/m^3, $\Delta t = 120$ μs and $j = 1.7 \times 10^7 A/m^2$. One square-shape pulse causes 0.0009465 °C temperature rising. This means that 100 Hz pulse frequency causes the temperature increment rate of 0.09 K/s. This is negligible in metallurgical processing. On the other hand, the current percolation might cause the heterogeneous temperature rising in the multiphase material. This has been examined in other cases for two-phase materials and found insignificant [42,44]. This has also been confirmed by experimental observations using OM and SEM in the present work, i.e., no trace of Ohm-heat-induced microstructure transformation has been observed.

Skin effect is another possible side effect that might affect the regeneration process. This is rather complicated for the materials containing two phases with vast difference of electrical and magnetic properties. In the present work, the magnetic permeability in ferrite phase is many times larger than that of austenite. No significant skin effect was observed for the samples processed in the present work.

There are still some open questions to be addressed in future research on both physical phenomena characterization and technical issue. For example, the Cr distribution in the samples after electropulsing treatment needs to be characterized by the APT, the formation and dissolution of G-phase under electropulsing treatment needs to be characterized, the aging behaviour of the regenerated samples need to

Table 5
Vickers micro-hardness (HV0.1) before and after electropulsing treatment.

Sample	D861		D989		D999		D979		D862	
	Before EP	After EP	Before EP	After EP	Before EP	After EP	Before EP	After EP	Before EP	After EP
Average	594	300	581	271	729	337	428	263	470	296
Top 15	628	348	595	318	795	414	512	279	534	331
Top 10	634	373	609	348	806	441	538	294	544	351

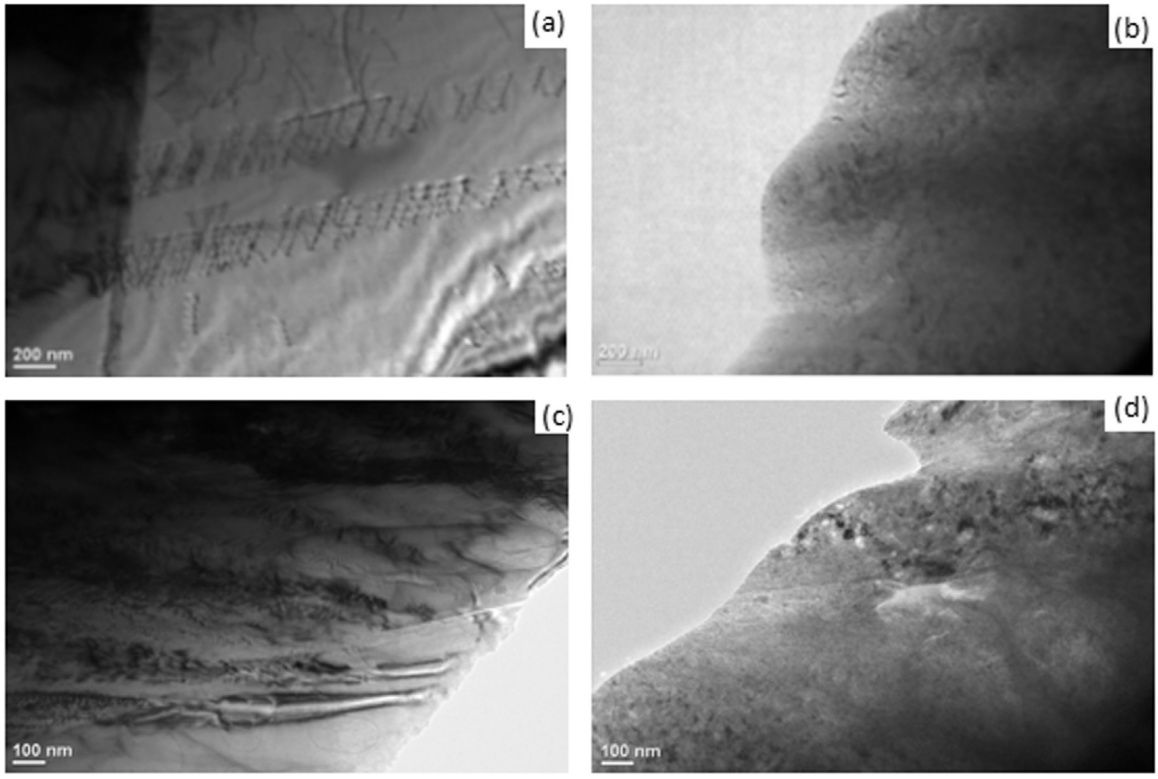

Fig. 6. TEM images for D979 sample: (a) and (c) are for the aged sample before electropulsing treatment; and (b) and (d) are for the aged sample after electropulsing treatment.

be investigated, the application of the electropulsing to other shape samples (e.g. cylinder pipes) needs to be explored. Some technical issues remain in scale-up from small specimens to real components, and further studies are necessary to push this technique to lower temperature treatment.

5. Conclusions

(1) A fast regeneration method has been developed to treat the aged duplex stainless steel charpy test specimens. According to the thermoelectric power measurement, one hour electropulsing treatment leads to the regeneration of > 83% of aged microstructure in terms of TEP characterization. The charpy impact toughness has been recovered significantly. The Vickers micro-hardness was also recovered to that of near to the unaged materials.
(2) The regeneration has not changed the microstructure in grain scale. OM, SEM and EBSD characterization shows no change of the grain morphology, configuration of phases and crystallographic texture in the samples after electropulsing treatment. It was the spinodal decomposition and early stage G-phase to be reversed by the electropulsing treatment. TEM indicates the change of dislocations but no trance of precipitates.
(3) The regeneration is due to the electric-current-induced reverse of system free energy sequence. The electric current free energy causes a significant change of free energy difference between the decomposed and un-decomposed microstructures, which drives the segregated alloying elements to be homogenized in the ferrite phase. The mechanical properties are hence to be regenerated.
(4) The Ohm heat in the regeneration treatment is negligible according to the calculation. The electropulsing enhanced mobility enables the regeneration to be completed in very short time duration.

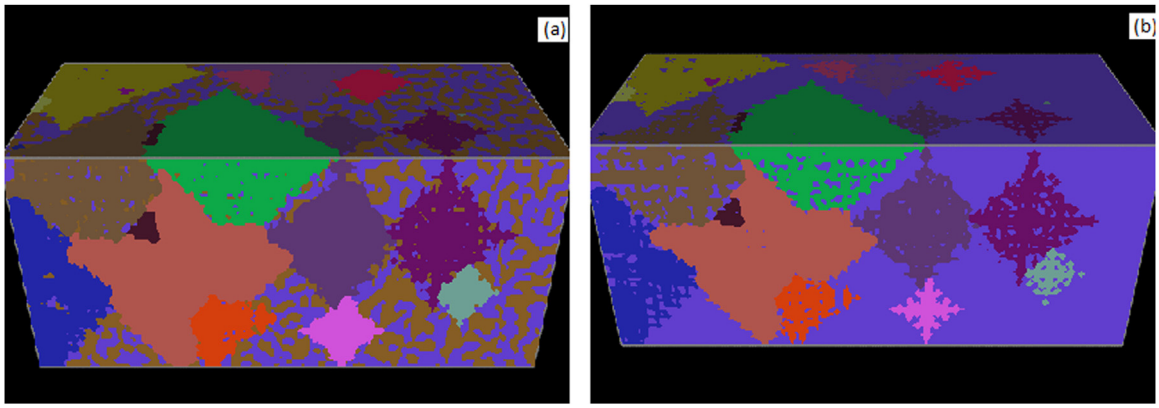

Fig. 7. Reconstructed microstructure for calculation of the Gibbs free energy due to electric current: (a) Aged structure with Cr decomposition in ferrite; (b) Cr are homogeneous in the ferrite phase after fully regeneration. The figures were generated by MatVisual code package.

Acknowledgements

The work was sponsored by Materials Aging Institute (MAI) at Electricité de France (EDF) within the MAI scientific network (MAI-SN) under the contract CLS-511-30. The authors are grateful to Dr. Shirley Northover at the Open University for fruitful discussions.

References

[1] L. Karlsson, H. Norden, Overview no. 63 non-equilibrium grain boundary segregation of boron in austenitic stainless steel-IV. precipitation behaviour and distribution of elements at grain boundaries, Acta Metall. 36 (1) (1988) 35–48.
[2] C.A. Schuh, T.C. Hufnagel, U. Ramamurty, Mechanical behaviour of amorphous alloys, Acta Mater. 55 (12) (2007) 4067–4109.
[3] M.F. Ashby, A.L. Greer, Metallic glasses as structural materials, Scr. Mater. 54 (3) (2006) 321–326.
[4] S.J. Zinkle, G.S. Was, Materials challenges in nuclear energy, Acta Mater. 61 (3) (2013) 735–758.
[5] J.B. Seol, J.G. Kim, S.H. Na, C.G. Park, H.S. Kim, Deformation rate controls atomic-scale dynamic strain aging and phase transformation in high Mn-TRIP steels, Acta Mater. 131 (1) (2017) 187–196.
[6] T. Sourmail, Precipitation in creep resistant austenitic stainless steels, Mater. Sci. Technol. 17 (1) (2001) 1–14.
[7] R. Takemoto, H. Mizubayashi, Effects of passing electric current on structural relaxation, crystallization and elastic property in amorphous Cu 50, Ti 50, Acta Metall. Mater. 43 (4) (1995) 1495–1504.
[8] L. Berthier, G. Biroli, Theoretical perspective on the glass transition and amorphous materials, Rev. Mod. Phys. 83 (83) (2010) 587–645.
[9] R.S. Qin, S.X. Su, J.D. Guo, G.H. He, B.L. Zhou, Suspension effect of nanocrystalline grain growth under electropulsing, Nanostruc. Mater. 10 (1) (1998) 71–76.
[10] Y.Y. Tu, X.H. Wang, H.L. Huang, X.F. Zhou, J.Q. Jiang, Effect of Si on the aging behavior of cold-drawn pearlitic steel wires, Metall. Mater. Trans. A 48 (2) (2017) 659–665.
[11] A.B. Pevtsov, V.Y. Davydov, N.A. Feoktistov, V.G. Karpov, Nanoscale-crystallite nucleation and growth in amorphous solids, Phys. Rev. B 52 (2) (1995) 955–966.
[12] Y. Onodera, K.I. Hirano, The effect of direct electric current on precipitation in a bulk Al-4 wt% Cu alloy, J. Mater. Sci. 11 (5) (1976) 809–816.
[13] Y. Onodera, Y. Onodera, Ph.D. Thesis, Tohoku University, 1991., Tohoku University, 1991.
[14] Y. Onodera, J.I. Maruyama, K.I. Hirano, Retardation of the precipitation reaction by d.c. stress in an Al-12.5 wt% Zn alloy, J. Mater. Sci. 12 (6) (1977) 1109–1114.
[15] N. Afify, A.F. Gaber, G. Abbady, Fine scale precipitates in Al-Mg-Zn Alloys after various aging temperatures, Mater. Sci. Appl. 2 (5) (2011) 427–434.
[16] T.J. Koppenaal, C.R. Simcoe, The effect of electric current on the aging of an Al–4%Cu alloy, Trans. Met. Soc. AIME 227 (1963) 615–617.
[17] H. Conrad, Electroplasticity in metals and ceramics, Mater. Sci. Eng. A 287 (2) (2000) 276–287.
[18] G.Q. Teng, Y.S. Chao, Z.H. Lai, L. Dong, A new method of nanocrystallization of Fe78B13Si9 amorphous alloy, Chin. Sci. Bull. 39 (1994) 974.
[19] Y.B. Jiang, G.Y. Tang, C.H. Shek, Y.H. Zhu, Z.H. Xu, On the thermodynamics and kinetics of electropulsing induced dissolution of β-Mg17Al12 phase in an aged Mg–9Al–1Zn alloy, Acta Mater. 57 (16) (2009) 4797–4808.
[20] W.J. Lu, X.F. Zhang, R.S. Qin, Stability of precipitates under electropulsing in 316L stainless steel, Mater. Sci. Tech. 31 (13) (2015) 1530–1535.
[21] R.S. Qin, A. Bhowmik, Computational thermodynamics in electric current metallurgy, Mater. Sci. Tech. 31 (13) (2015) 1560–1563.
[22] R.S. Qin, S.X. Su, Thermodynamics of crack healing under electropulsing, J. Mater. Res. 17 (8) (2002) 2048–2052.
[23] J.D. Mithieux, R. Fourmentin, 475 °C embrittlement in duplex: a review, in Duplex stainless steel, Conference Proceedings, 2010.
[24] C. Pareige, S. Novy, S. Saillet, P. Pareige, Study of phase transformation and mechanical properties evolution of duplex stainless steels after long term thermal ageing (> 20 years), J. Nucl. Mater. 411 (1) (2011) 90–96.
[25] C. Pareige, M. Roussel, S. Novy, V. Kuksenko, P. Olsson, C. Domain, P. Pareige, Acta Mater. 59 (6) (2011) 2404–2411.
[26] J. Emo, C. Pareige, S. Saillet, C. Domain, P. Pareige, Kinetics of secondary phase precipitation during spinodal decomposition in duplex stainless steels: a kinetic Monte Carlo model – comparison with atom probe tomography experiments, J. Nuc. Mater. 451 (1–3) (2014) 361–365.
[27] X.F. Zhang, W.J. Lu, R.S. Qin, Removal of MnS inclusions in molten steel using electropulsing, Scr. Mater. 69 (6) (2013) 453–456.
[28] A. Rahnama, R.S. Qin, Electropulse-induced microstructural evolution in a ferritic–pearlitic 0.14% C steel, Scr. Mater. 96 (2015) 17–20.
[29] Y. Matsukawa, T. Takeuchi, Y. Kakubo, T. Suzudo, H. Watanabe, H. Abe, T. Toyama, Y. Nagai, The two-step nucleation of G-phase in ferrite, Acta Mater. 116 (2016) 104–113.
[30] K.H. Lo, C.H. Shek, J.K.L. Lai, Recent developments in stainless steels, Mater. Sci. Eng. R. 65 (4) (2009) 39–104.
[31] M. Tane, T. Ichitsubo, H. Ogi, M. Hirao, Elastic property of aged duplex stainless steel, Scr. Mater. 48 (3) (2003) 229–234.
[32] Y.S. Yi, T. Shoji, Detection and evaluation of material degradation of thermally aged duplex stainless steels: electrochemical polarization test and AFM surface analysis, J. Nucl. Mater. 231 (1–2) (1996) 20–28.
[33] N. Maeda, T. Goto, T. Kamimura, T. Naito, S. Kumano, Y. Nakao, Changes in electromagnetic properties during thermal aging of duplex stainless steel, Inter. J. Pre. Ves. Pip. 71 (1) (1997) 7–12.
[34] Y. Kawaguchi, S. Yamanaka, Mechanism of the change in thermoelectric power of cast duplex stainless steel due to thermal aging, J. Alloy. Comp. 336 (1) (2002) 301–314.
[35] J.S. Cheon, I.S. Kim, Evaluation of thermal aging embrittlement in CF8 duplex stainless steel by small punch test, J. Nucl. Mater. 278 (1) (2000) 96–103.
[36] M.D. Mathew, L.M. Lietzan, K.L. Murty, V.N. Shah, Low temperature aging embrittlement of CF-8 stainless steel, Mater. Sci. Eng. A 269 (1–2) (1999) 186–196.
[37] P.D.S. Pedrosa, J.R. Teodosio, S.S.M. Tavares, J.M. Neto, M.R. da Silva, Magnetic and mechanical hardening of Fe-based alloys, J. Alloy. Comp. 329 (1–2) (2001) 114–117.
[38] S.S.M. Tavares, M.R. da Silva, J.M. Neto, Magnetic property changes during embrittlement of a duplex stainless steel, J. Alloy. Comp. 313 (1–2) (2000) 168–173.
[39] C.H. Shek, Growth of α′ clusters and associated changes in magnetic properties in a duplex stainless steel, Phys. Stat. Sol. A 186 (1) (2001) R7–R9.
[40] A. Rahnama, R.S. Qin, Room temperature texturing of austenite/ferrite steel by electropulsing, Sci. Rep. 7 (2017) 42732.
[41] R.S. Qin, E.I. Samuel, A. Bhowmik, Electropulse-induced cementite nanoparticle formation in deformed pearlitic steels, J. Mater. Sci. 46 (9) (2011) 2838–2842.
[42] R.S. Qin, Electric-field-induced alignment of electrically neutral disk-like particles: modelling and calculation, Sci. Rep. 7 (2017) 8449.
[43] K.L. Weng, H.R. Chen, J.R. Yang, The low-temperature aging embrittlement in a 2205 duplex stainless steel, Mater. Sci. Eng. A 379 (1–2) (2004) 119–132.
[44] R.S. Qin, Using electric current to surpass the microstructure breakup limit, Sci. Rep. 7 (2017) 41451.
[45] U. Bohnenkamp, R. Sandström, G. Grimvall, Electrical resistivity of steels and face-centered-cubic iron, J. Appl. Phys. 92 (8) (2002) 4402–4407.
[46] S.M. Thompson, B.K. Tanner, The magnetic properties of pearlitic steels as a function of carbon content, J. Magn. Magn. Mater. 123 (3) (1993) 283–298.
[47] R.S. Qin, E.R. Wallach, A phase-field model coupled with a thermodynamic database, Acta Mater. 51 (20) (2003) 6199–6210.
[48] R.S. Qin, H.K.D.H. Bhadeshia, Phase-field model study of the effect of interface anisotropy on the crystal morphological evolution of cubic metals, Acta Mater. 57 (7) (2009) 2210–2216.
[49] R.S. Qin, H.K.D.H. Bhadeshia, Phase-field model study of the crystal morphological evolution of hcp metals, Acta Mater. 57 (11) (2009) 3382–3390.